IEEE Access
Multidisciplinary | Rapid Review | Open Access Journal

Received 13 July 2024, accepted 27 July 2024, date of publication 12 August 2024, date of current version 17 September 2024.

Digital Object Identifier 10.1109/ACCESS.2024.3442016

APPLIED RESEARCH

Unveiling Insights Into Partial Discharge and Design and Encapsulation Challenges in DCB-Based Power Converters for Aerospace Applications

TOHID SHAHSAVARIAN[1], (Member, IEEE), MORITZ PLONER[2], (Graduate Student Member, IEEE), KERRY LYNN DAVIS-AMENDOLA[3], (Graduate Student Member, IEEE), BRIAN CHISLEA[4], JOHN MCKEEN[4], DI ZHANG[5], (Fellow, IEEE), ANDREA CAVALLINI[2], (Fellow, IEEE), AND YANG CAO[3], (Senior Member, IEEE)

[1]Applied Technology Services, Pacific Gas and Electric, San Ramon, CA 94583, USA
[2]Electrical, Electronic and Information Engineering Department, University of Bologna, 40136 Bologna, Italy
[3]Department of Materials Science and Engineering, University of Connecticut, Storrs, CT 06269, USA
[4]Dow Inc., Midland, MI 48642, USA
[5]Department of Electrical and Computer Engineering, Naval Postgraduate School, Monterey, CA 93943, USA

Corresponding author: Yang Cao (yang.cao@uconn.edu)

This work was supported in part by the National Aeronautics and Space Administration (NASA), and in part by the U.S. Navy under Grant N00244-20-1-0008.

ABSTRACT This study combines comprehensive analyses of design parameters with encapsulation solutions of Direct Copper Bond (DCB) substrates used in high voltage power converter modules, focusing on partial discharge (PD) activity under varying pressures for aerospace applications. A detailed PD investigation on triple junction points as the main culprit of the failure in power electronics was conducted, and the design and material aspects through experimental and simulation analysis were examined. PD initiation and extracted information are presented for three common pad geometries on two types of substrates (AlN and G-10/FR4). The results reveal better performance of the AlN that has higher permittivity, i.e., 20-30% and 10-20% higher PD inception voltage (PDIV) than G-10/FR4 at ambient and low pressures, respectively, and 40-65% lower PDIV at low pressures due to the higher rate of gas ionization compared to the ambient pressure. The study also explores the impact of pad geometric design such as corner smoothness and spacing on electric field intensity, with an introduced pressure- and temperature-dependent ionization model coupled with 3D finite element model to quantify the impact of the pressure on the gas ionization and PD initiation. Furthermore, an extensive experimental and numerical study of PD on liquid and gel encapsulated DBC substrates at ambient and low pressures was also conducted. Two silicone gels (Dowsil^{TM} 3-4170 and Sylgard^{TM} 527) and one refrigerant dielectric liquid (fluorinert FC40) were investigated as encapsulating dielectrics for high voltage applications. The results reveal that different silicone gels, despite similar dielectric properties, can exhibit drastically different PD resistance due to intrinsic bulk properties and self-healing capabilities, outperforming liquid-based encapsulants. This highlights the significance of dielectric fluid and gel insulations characteristics to the performance of HV modules for aerospace applications.

INDEX TERMS Aerospace application, direct copper bond (DCB) substrate, electrical insulation, encapsulation, fluorinert, high power converters, partial discharge (PD), silicone gel.

I. INTRODUCTION

The successful transformation towards pure electric vehicles enkindles the endeavor to develop full electric airplanes that

The associate editor coordinating the review of this manuscript and approving it for publication was Ravi Mahajan.

go beyond the more-electric aircraft (MEA) with promise of fuel consumption reduction of up to 25% [1], [2]. Despite the introduction of different robust architecture and electrical interconnection topologies for parallel/series hybrid and electric propulsions, the significant power and energy requirements of commercial and long-range airplanes raise the concerns and technology challenges of three main subsystems: energy generation and storage, electrical machines, and power electronics [3]. Different technologies of power switching transistors, especially the wide-bandgap (WBG) semiconductors such as Gallium Nitride (GaN) and Silicone Carbide (SiC) provide largely expanded ranges of operating frequency, voltage, temperature, and current for the fast-growing markets [4], [5]. Miniaturization and high-power demands for efficient, compact, and reliable system design necessitate the special dielectric encapsulation treatment of the electronic module packages to protect the power modules against environmental and electrical stresses, as well as degradation and premature failure.

In a real operating condition, the triple junction points where the metalized conductors, substrate, and encapsulating medium meet is where the higher electrical stresses lead to PDs and degradation of the insulation [6], [7]. The harsh environmental condition facilitates the initiation of the discharges in these weak areas. Direct bonded copper to dielectric substrates often with high thermal conductivity is a widely used and time-tested technology for the main structure of electronic boards in power electronics with strong high voltage withstand while providing high thermal conduction and heat dissipation. In this design, two dissimilar electronic materials, i.e., copper and ceramic, are directly bonded and the copper pads are soldered to the transistor terminals. Different electrode designs are applied based on the operating conditions and converter technology to ensure efficient heat dissipation, optimal current flow, minimal losses, robustness, and ease of integration [8], [9], [10]. Therefore, a detailed study of the impact of different design parameters on PD activity at varying environmental conditions is of the utmost importance in the manufacturing process of the power electronic packaging for aerospace applications.

On the other hand, for effective encapsulation of the electronic components without imposing further mechanical forces on the bonding wires and weakly soldered terminals, liquid and semi-solid forms of dielectric materials are introduced. The cross-linked adhesive and resilient gels that have physical properties between liquid and solid provide a more benign packaging solution compared to the liquids. Pros and cons of using gels compared to liquids including the claimed self-healing property or irreversible permanent damage of the gels due to the high electrical stresses in high power devices are arguable. However, the consequential degradation of the dielectric material and higher electrical stresses due to the formation of the voids from locally ignited PDs cannot be overlooked. Not only voids and electrical trees are present inevitably inside the solid and liquid dielectrics, the occurrence of PD has been reported as another cause of the formation of these voids inside the gel along the tree propagation. Salvatierra et al. [11] have studied the impact of different mixing ratios of the transparent liquid components for two commercially available cross-linking gels in terms of the presence and rate of collapse of the bubble-shaped cavities attached to the filamentary branched electrical trees inside the gel. However, they pointed out that the electron injection at the branch tips more specifically might be considered the dominant factor causing the liquid phase of the cured gel to heat up, vaporize, and form the bubbles. Also, Mancinelli et al. [12] have discussed the impact of space charge injection on tree propagation inside the silicone gel at different voltage waveforms and frequencies. Experimental motion observations reported by Nakamura [13] and viscoelastic analysis of Sato et al. [14] from the same research group showed the impact of the frequency, rise time, and polarity of the voltage impulse as well as the charge accumulation and surface conductivity on the void shape along the discharge tracks across the solid dielectric surface enclosed with the gel. Besides the abovementioned PD impact on the void formation inside the gel, Semenov et al. [15] have investigated the impact of bipolar and unipolar square voltage waves on the charge memory effect of voids introduced to the silicone liquid as an alternative to the silicone gel. In addition to these works, a few PD studies have been conducted on different types of dielectric liquids (such as mineral and synthetic oils, Novec, and fluorinert fluids [16], [17], [18]) to represent the capability of these dielectrics in protecting the electronic board ''at ambient conditions''.

The vulnerability of the dielectric encapsulants to PDs as revealed by prior research can be further intensified by impurities in power modules under high voltage applications. Bear in mind that these key devices are used to interconnect both AC and DC subsystems and to protect the DC loads in hybrid and electric aircraft, so their safe operation under high voltages and harsh environmental conditions have not been fully validated. Our prior experimental studies on commercially available high voltage/high current power modules indicated the risks of untimely initiation of the PDs at low pressures and high temperatures in the operating range of the modules, and the insufficient safe margin of these components for aerospace applications [19].

The aim of this study is to systematically and comprehensively evaluate the performance of power electronic modules in relation to partial discharge activity and high-altitude operation. Our analysis commences with a detailed exploration of various influencing design factors and material selections, including the dielectric/ceramic insulator, bonded copper onto the substrate, following by delving into PD resistance performance of gel/liquid-based insulation encapsulants and PD source identification. The effect of pressure on PD initiation in encapsulated samples using two different silicone gels, Dowsil^{TM} 3-4170 (abbreviated as SiG 4170) and Sylgard^{TM} 527 (abbreviated as SiG 527), and one

refrigerant dielectric liquid, Fluorinert FC40, across different designs is investigated and discussed.

The results show that encapsulating the DCBs can effectively increase PDIV by 15% to 50%. However, four major factors—encapsulating material, operating pressure level, dielectric substrate, and pad shape—play a crucial role in defining the amount of PDIV variation for the modules. AlN substrates exhibit 10% to 55% higher PDIV compared to G10/FR4 substrates, with a greater difference observed at lower pressures. When the pressure is reduced to 20 and 10 kPa, the PDIV decreases on average by 25% and 35% for fluoroinert-encapsulated samples and by 25% to 45% for silicone gel-encapsulated samples compared to ambient conditions. Comparing different silicone gel materials is complex, as factors such as gel cross-linking, hardness properties, and adhesiveness must be carefully evaluated. This study shows that SiG 527 has 15% to 75% higher PDIV than SiG 4170, depending on the pressure and DCB configuration.

This assessment aims to evaluate the altitude readiness of commercial power modules and commonly used encapsulation materials, considering the aforementioned factors through thorough analysis. Detailed technical specifications of the selected materials are provided in Section II. Additionally, the general properties and intrinsic characteristics of the two liquid and gel-based encapsulants used in power converter modules, which are studied in this paper, are illustrated below.

A. SILICONE GEL

This special class of encapsulants is formed via the cross-linking process of two different chemical groups: vinyl end-terminated polymers and silane group carried by functional oligomers. Wide bond angle and free bond rotation between the silicon and oxygen atoms result in high flexibility of the polymer chain, high free volume, and in turn softness of the chemical compound [20]. Generally, two transparent liquid reaction components are mixed in a 1:1 ratio, then degassed, and cured at a specific temperature. Silicone gel has high chemical, thermal, and electrical stabilities over a wide range of temperatures −45°C to 200°C beyond the maximum operating temperature of the electronic and semiconductor components. Great adhesion of the gel to the electronic components without imposing undesirable mechanical stresses on the connections as well as the self-healing quality of the gel against physical and electrical damages makes it a competent dielectric form of encapsulant for the power modules. However, different commercial components each with its own distinctive electrical, chemical, and thermal properties present varying capabilities against the PDs under harsh environmental conditions.

B. FLUORINERT

Different variants of perfluorinated compounds (PFCs) have been used as effective electronic refrigerant liquids, i.e., the emerging passive two-phase immersion cooling of data-center servers. They generally have a lower boiling point than silicone gels which depends on the molecular formulations. The main features of these electrical insulation and stable fluids are high dielectric strength, non-flammability and non-corrosiveness, and good compatibility. Test results reported in [17] by Fabian et al. show a higher potential gradient, and consequently, a higher electric field intensity in their simulated AlN power module substrate encapsulated with fluorinert compared to silicone gel and Novec fluid (HFE-7500). Also, Xu et al. [21] have presented the PDIV values for fluorinert at liquid and boiling conditions which shows the bubbles at boiling condition repel from the strong electric field area due to the dielectrophoretic force. Therefore, in our study, it was expected the possible bubbles generated around the pads at low pressures and the ambient temperature does not have a significant impact on the PDIV values compared to the silicone gel, and the test results can provide a clear impact of the altitude/pressure on the PDIV values for silicone gel compared to the fluorinert fluid.

II. EXPERIMENTAL SAMPLE DESIGN AND TEST FRAMEWORK

A. TEST SAMPLES AND MATERIALS

In this study, we have designed three main types of conductive pad structures, using the copper foils attached to the top of the substrate, which represents the different possible weak areas between them on electronic modules. The sample design layout is shown in Fig. 1. The width and thickness of each copper pad are 1.5 cm and 60 μm, and they are separated by 2 or 4 mm. Also, the backside of the substrates is covered with a copper clad. The same geometry was designed with sharp and round (radius curvature of around 1.5 mm) edges. Hereinafter, the denotation of A_B_C will be used to define each specific configuration where A is the geometry (LS, RS, or RR as given in Fig. 1), B is the edge shape (s for sharp and r for round), and C is the distance between the pads (2 or 4 mm). For example, LS_r_2 is the denotation of the geometry shown with a dashed blue squared area in Fig. 1.

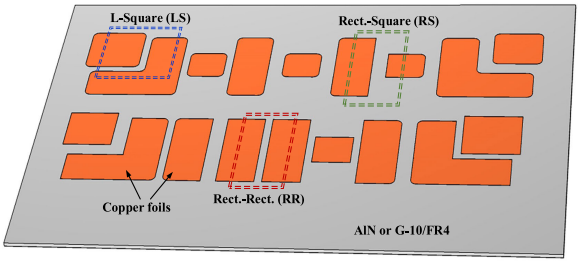

FIGURE 1. Design of the test sample for different geometries.

The base substrates studied in this paper are aluminum nitride (AlN) and glass-reinforced epoxy resin laminate (G-10/FR4) with the same thickness of 1.5 mm. The ceramic has been widely used in power modules because of its high thermal conductivity and FR4 is the commonly used solid material in printed circuit board (PCB) fabrication because of

TABLE 1. Electrical and thermal properties of substrates.

Properties	AlN	G-10/ FR4
Thermal conductivity [W m^{-1} K^{-1}]	170-220*	0.29
Maximum Operating Temperature [K]	973	538
Coefficient of Thermal Expansion [1/K]	4.5×10^{-6}	9.9×10^{-6}
Dielectric Constant at 1MHz	9	5
Dissipation Factor at 1MHz	0.0003	0.019
Breakdown Voltage [kV/mm]	15	31

* [22]

its good electrical insulation property between the copper layers minimizing interferences and supporting signal integrity. Their main electrical properties have been summarized in Table 1.

Additionally, two different brands of two-part silicone gels (DowsilTM 3-4170 and SylgardTM 527), as well as a fluorinert fluid (FC40) were obtained from the Dow Chemical Company and 3M, respectively. Note that, comparing these two specific silicone gel products, the overall hardness of each is an indicator of the level of cross-linking and inversely the level of the anticipated self-healing quality. Sylgard 527 is slightly harder than Dowsil 3-4170, therefore more crosslinked.

The main properties of these dielectric materials are given in Table 2. The selected silicone gels (after screening tests of many gels) have high dielectric strength, extreme stress relief property, low viscosity, as well as a good performance at low pressures, which make them the best options for our study. Fluorinert, with an average dielectric strength compared to the gel samples, has lower dielectric constant and higher volume resistivity.

TABLE 2. Technical data of the dielectric materials used in this study.

	Dowsil™ 3-4170	Sylgard™ 527	Fluorinert FC40
Viscosity (cP)	425	465	4.1
Dielectric Strength (kV/mm)	20	17	18
Dielectric Constant	2.85	2.85	1.9
Volume Resistivity (Ω.cm)	9.5×10^{14}	2.75×10^{15}	4×10^{15}
Dissipation Factor -at 100Hz -at 100kHz	0.0016 0.00007	0.002 0.0001	Not reported in
Operating Temperature (˚C)	-45 to 200	-45 to 150	-40 to 140 (165 boiling temp)

The DBC substrates designed for this study are made of two different base dielectric materials (AlN and G-10/FR4) and three different pad geometries (i.e., L-square (LS), rectangle-rectangle (RR), and rectangle-square (RS) shapes). They are designed on the top surface of the solid dielectric base plates, with and without back side uniform ground pad, as introduced earlier. The test voltage was applied between the pads through the soldered insulated wires to the pads. The containers including the test sample were filled with silicone gel/fluorinert and went through the degasification and curing processes before the tests.

B. ENCAPSULATION AND CROSS-LINKING PROCESSES

In order to effectively apply the well-mixed silicone gel to the components, while avoiding the formation of bubbles and thermal expansion of the mixed encapsulant inside the container during curing, the following steps were followed and are recommended:

- The substrate is well attached to the container to avoid creating any gaps between them, or a uniform gap between them, to be considered to allow the gel to flow and fill the gaps under the substrate.

- The dispensing gun and mixing nozzle are used for efficiently mixing of the two-part component without bubble formation as suggested by the manufacturer.

- For an effective curing process of the gels and to reduce the chance of bubble formation under low pressures, one extra step of curing at low pressure might be needed in addition to the guidelines provided by the manufacturer.

- If needed and suggested by the manufacturer, compatible primer coating should be applied to the substrate and copper pads before dispensing the silicone gel to ensure proper attachment of the gel to the substrate.

For each encapsulant, the following specific steps were taken:

• *Fluorinert FC40*: The test sample was degassed at room temperature under 2kPa for 15 minutes.

• *Dowsil 3-4170*: The encapsulated sample was degassed at room temperature under 2kPa for 15 minutes. The first step of curing was performed at 60°C and 20kPa for 30 minutes. The final curing step was at ambient pressure under 100°C for 10 minutes.

• *Sylgard 527*: The first step was degassing at room temperature under 2kPa for 15 minutes. The final curing step was at ambient pressure under 125°C for 2 hours.

C. TEST SETUP AND PROCEDURE

The PD tests were conducted inside a Faraday cage based on the circuit design introduced by IEC 60270. It provides highly sensitive detection capability (as low as 2pC) using a wide bandwidth data acquisition unit (16kHz-48MHz in addition to a 2.5MHz high pass software filter). The voltage was applied to different pad geometries through the soldered insulated wires to the copper foils. The test sample was connected in parallel with the coupling capacitor and measuring impedance needed to complete the sensing circuit loop for generated PD pulses. In order to perform the tests at low pressures, the samples were placed inside a low-pressure chamber connected to a mechanical pump. Fig. 2 shows a complete circuit design for the PD test in this study.

III. EXPERIMENTAL ASSESSMENTS AND TEST RESULTS

A. GEOMETRIC PAD DESIGN AND SUBSTRATE MATERIAL EXAMINATION FOR PD INITIATION

The PD tests for each group of the geometries designed on both types of substrates were performed at three pressure levels, i.e., 100 kPa, 20 kPa, and 10 kPa, corresponding

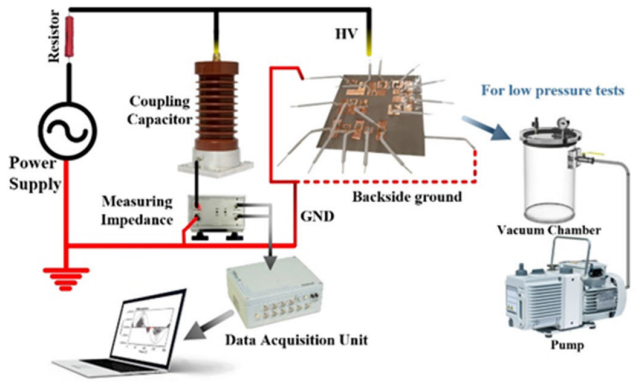

FIGURE 2. PD test setup for DBC board study at different pressures.

to the pressures at sea and the altitudes of around 38 kft (11.6 km) and 52 kft (15.8 km), respectively. It is expected that the power modules experience these pressure levels in commercial airplanes during stable cruise mode for a considerable period of time after takeoff. The AC voltage with an increasing rate of 100 V/s was applied between the pads until a consistent and stable PD activity is detected. In addition to the PDIV and its corresponding phase resolved PD (PRPD) pattern, the voltage was increased to record surface flashover voltage. These values are presented in the figure with a bar with a gradient color from a bright low value (PDIV) to a dark high value (flashover voltage). In some cases, at low pressure, especially at 10 kPa, the flashover occurs at low voltages before detecting the PDIV which is shown with a short black bar in the plots. The test for each type of design and scenario was repeated up to five times on new samples to obtain consistent results to represent the statistical plots.

1) L TO SQUARE (LS) PAD CONFIGURATION

Fig. 3 shows the PD and flashover voltage values recorded for LS configuration at different pressures. As can be seen, at low pressures, the chance of flashover is high, even with only a small voltage rise above PDIV. Also, slightly higher values for PD and flashover were recorded for AlN substrate. To better clarify and discuss the abovementioned parameters in the plots, the results of the tests were presented for the LS configuration with only sharp edges. Fig. 4 represents a comparison between the results obtained for the same geometry with and without backside ground (BSG) connection for AlN substrate as the main material used in the commercially available power modules. It shows a significant impact of the ground connection on early initiation of PD at different pressures. The location of the PDs and flashovers are presented in the next section.

2) RECTANGULAR TO RECTANGULAR (RR) PAD CONFIGURATION

This geometry represents a uniform electric field distribution where the edges are expected to be the weak points. Therefore, Fig. 5 presents the PD test results for both sharp and

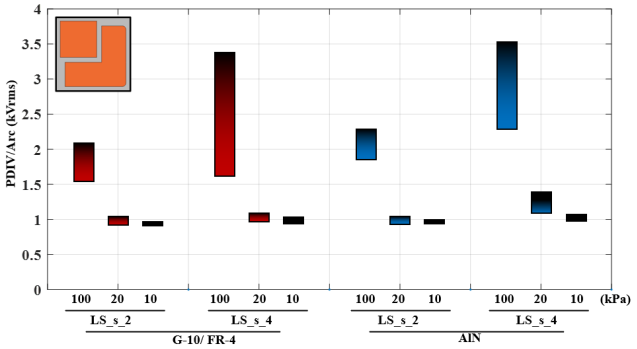

FIGURE 3. PD test results for LS configuration and both substrates at different pressures (without BSG connection).

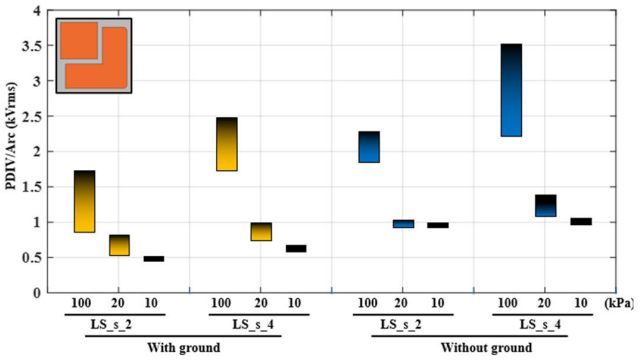

FIGURE 4. Comparison between the PD test results for LS configuration on AlN substrate with (yellow color bars) and without (blue color bars) BSG connection.

round edge corners for the distance of 2 and 4mm between the pads. The distance has a significant impact on the flashover voltage at ambient pressure, unlike its negligible impact on PDIV values. However, both PD and flashover voltages are significantly decreased at low pressures. The corner smoothness does not affect the results at low pressures, unlike the changes observed at ambient pressure.

Fig. 6 shows the impact of the BSG connection on the results. When BSG is connected, both PDIV and flashover voltages are noticeably decreased. Also, the impact of the edge shape at ambient pressure is more obvious in a connected BSG configuration due to the higher intensity of the electric field around the sharp edges.

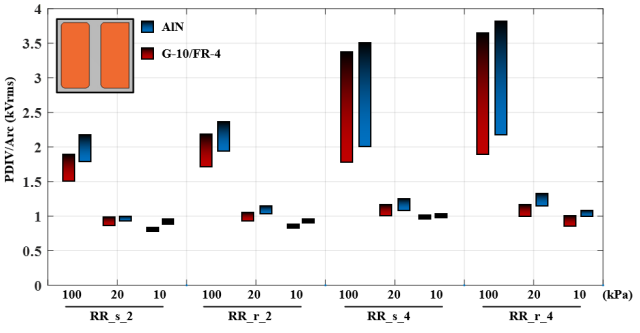

FIGURE 5. PD test results for RR configuration and both substrates at different pressures (without BSG connection).

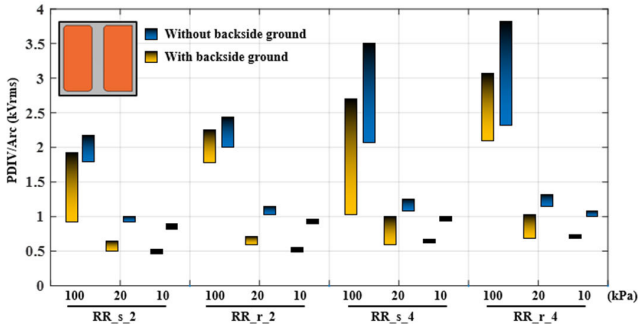

FIGURE 6. Comparison between the PD test results for RR configuration on AlN substrate with (yellow color bars) and without (blue color bars) BSG connection.

3) RECTANGULAR TO SQUARE (RS) PAD CONFIGURATION

This pad geometry represents a smaller impact area between the pads; however, the small square pad increases the electric field non-uniformity and decreases the PDIV values. On the other hand, there is longer distance between the edges of two pads which carries a higher weight on the PD results. Therefore, the test result values presented in Fig. 7 for RR geometry is higher compared to the RR geometry shown in Fig. 5. Also, same as the previous geometries, the PDIV and flashover values for AlN is higher than G-10/FR4 substrate.

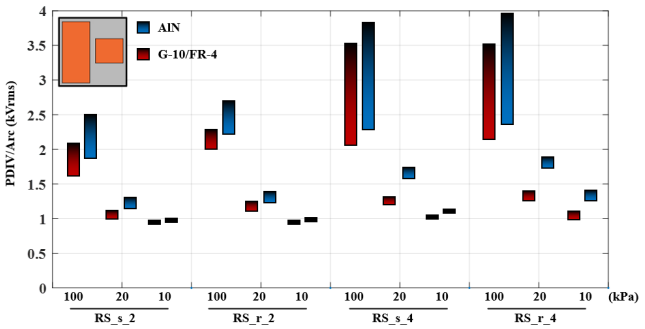

FIGURE 7. PD test results for RS configuration and both substrates at different pressures (without BSG connection).

As expected from the previous test results, Fig. 8 shows a considerably lower PDIV and flashover values for the sample with BSG connection.

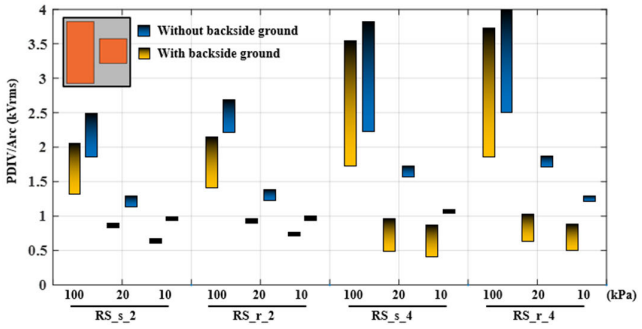

FIGURE 8. Comparison between the PD test results for RS configuration on AlN substrate with (yellow color bars) and without (blue color bars) BSG connection.

B. ASSESSMENT OF ENCAPSULANT EFFICACY FOR PD MITIGATION

After sample preparation and gel temperature equilibrium per proposed encapsulation instruction in section II-B, the pressure inside the vacuum chamber was adjusted to the desired value and PD test was performed on each prepared sample at different pressures. Unlike the test results presented in III-A, the voltage was not increased beyond the inception voltage to avoid any permanent damage to the silicone gels due to the possible flashover incident. The test for each type of design and scenario was repeated five times to obtain the statistical data of the results.

1) FLUORINERT ENCAPSULATION OF AlN BASE SUBSTRATE

The impact of fluid encapsulation on the PD initiation of three pad designs on AlN substrate was investigated under different pressures. Fig. 9 shows the PDIV as a consequence of the high tangential field between the pads separated with a distance of either 2 or 4 mm without the substrate's backside ground (BSG) connection. The test results for round-edge pads are presented throughout this study; however, approximately 3-8% lower PDIV values were recorded for sharp edge compared to round edge pad design. The results in Fig. 9 show that, compared to the ambient pressure, there is a 15-35% and 27-52% reduction of PDIV under 20kPa and 10kPa, respectively.

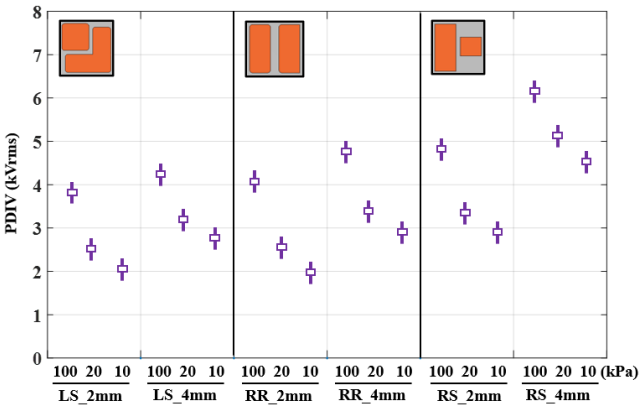

FIGURE 9. Measured PDIV values for three round-edge pad geometries with the fluorinert encapsulation without back side AlN substrate grounding with different distances under different pressures.

The PDIV values for the different geometries and pressures with BSG connection are given in Fig. 10. It shows a significant reduction of the PDIV (20-45%) compared to the previous test configuration without BSG. Also, compared to ambient pressure, a 23-27% and 30-36% reduction of PDIV under 20kPa and 10kPa is observed, respectively.

2) SILICONE GEL ENCAPSULATION OF AlN BASE SUBSTRATE

Separate samples were designed and encapsulated with two different silicone gels following the procedure described in section II-B. Figs. 11-13 show the recorded PDIV values for encapsulated three different pad designs. The impact of the

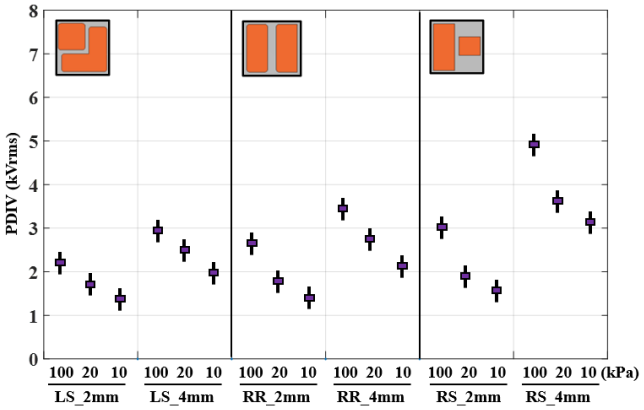

FIGURE 10. Measured PDIV values for three round-edge pad geometries with the fluorinert encapsulation with back side AlN substrate grounding with different distances under different pressures.

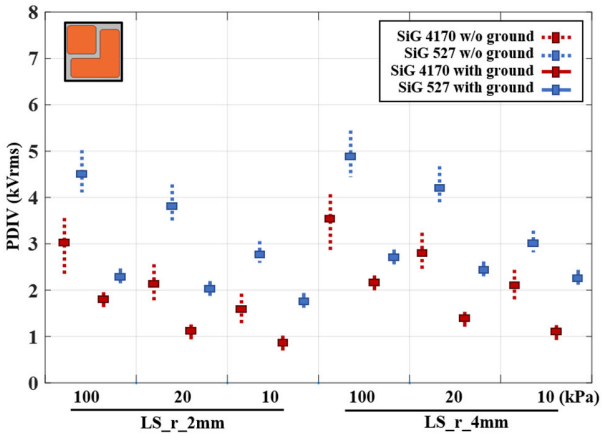

FIGURE 11. Measured PDIV values for encapsulated round-edge LS pad geometry with two different types of silicone gel with and without back side AlN substrate grounding with different distances under different pressures.

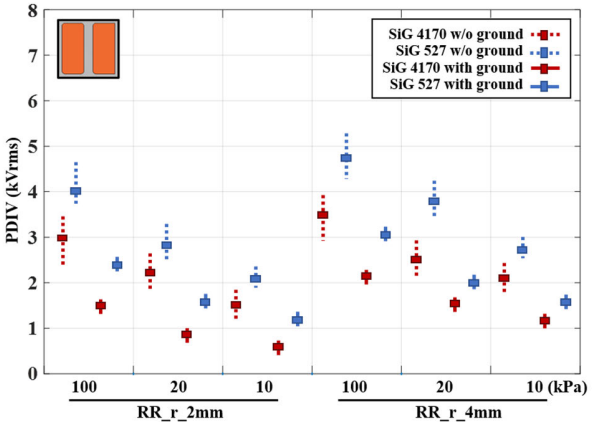

FIGURE 12. Measured PDIV values for encapsulated round-edge RR pad geometry with two different types of silicone gel with and without back side AlN substrate grounding with different distances under different pressures.

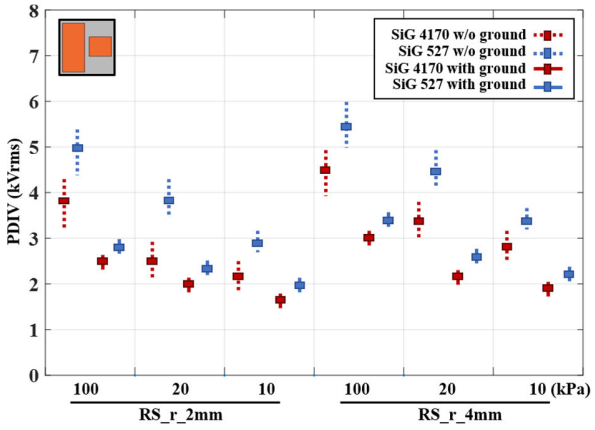

FIGURE 13. Measured PDIV values for encapsulated round-edge RS pad geometry with two different types of silicone gel with and without back side AlN substrate grounding with different distances under different pressures.

pressure, distance, BSG connection, and applied gel on the PDIV values are presented in these plots. It is important to note that the wider variation in the PDIV values in these plots compared to the results presented for fluorinert-encapsulated samples is due to the higher likelihood of stable bubble formation as pressure drops to 20 and 10 kPa. Although the introduced cross-linking process ensures achieving a bubble-free encapsulated sample, the formed bubbles at low pressures, especially at 10kPa, can take up to 12 hours to clear after pressure rises to 100kPa.

The major observations from the results are as follows:

- The PDIV values for SiG 527 are approximately 15-75% higher than SiG 4170 with and without considering the BSG connection under different pressures.
- On average, the PDIVs at 20 and 10 kPa are 15-35% and 35-50% lower than the PDIVs at ambient pressure, 100kPa. This range of recorded inception values does not show a significant dependency on the type of gel, pad shape, or BSG connection. In other words, the impact of pressure on the PDIV values is consistent.
- Also, the PDIV values for samples with BSG connection were mainly 30-50% lower than the samples without BSG connection. Less variation in the PDIV results was obtained for the samples with BSG compared to without BSG connection.
- 10-30% higher PDIV was recorded for the pads with 4mm compared to 2mm gap for all designs, and this difference does not depend on the pressure, or type of applied gel. However, it is expected to observe the impact of pressure on this difference when the gels are not properly cured and a high number of bubbles are produced at low pressures.

3) SILICONE GEL ENCAPSULATED SAMPLES WITH AlN SUBSTRATE VERSUS G10/FR4 SUBSTRATE

Two commonly used insulation substrates for electronic design, AlN and G10/FR4, of equal thickness were selected and encapsulated with the silicone gels introduced in this paper. Fig. 14 shows the PDIV values obtained for three different pad designs on these substrates with two different types of silicone gel encapsulations.

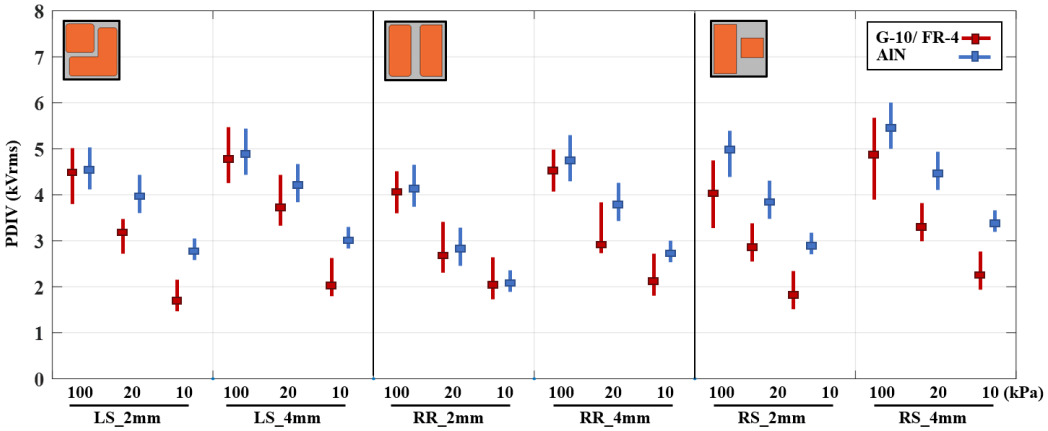

FIGURE 14. Measured PDIV values for encapsulated AlN and G10-FR4 with silicone gel B for different geometries with different distances under different pressures without BSG.

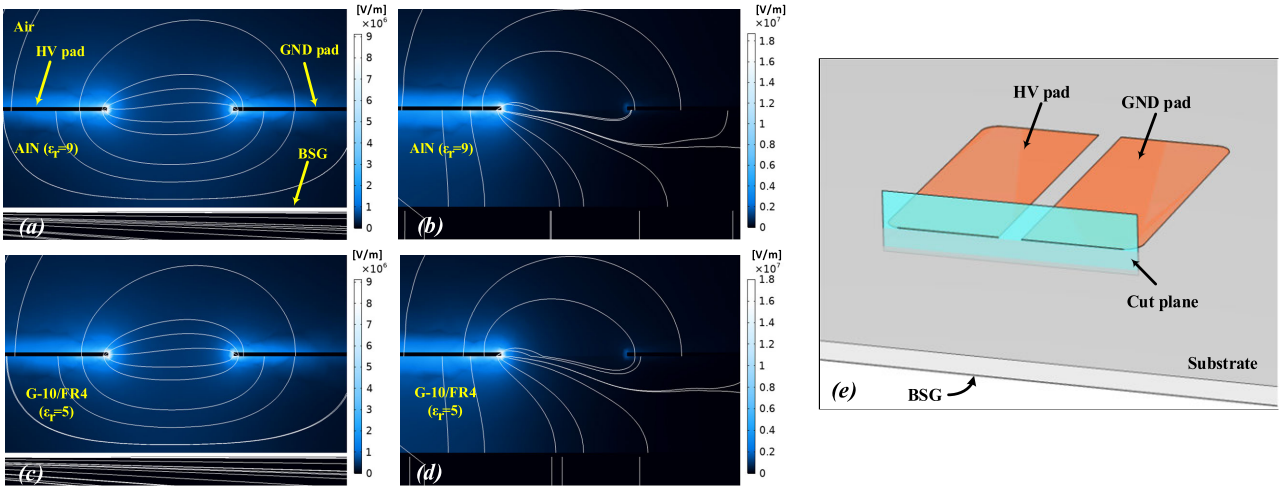

FIGURE 15. Cross section view of the electric field intensity and distribution lines between the RR pads inside the cut plane for the substrates: AlN (a) without and (b) with BSG; and G-10/FR4 (c) without and (d) with BSG for the geometry given in (e).

Generally, the results show 10-50% lower PDIV values for G-10/FR4 compared to the AlN. The impact of the substrate on the results is more apparent when the distance between the pads increases. The tangential field generated between the pads where the voltage is applied is more electrically stressful when the bubbles form especially at low pressure. Therefore, a significant PDIV drop is observed at lower pressures (almost 30% and 50% lower PDIV at 20 and 10kPa compared to 100kPa, respectively) for both substrates.

IV. PRELIMINARY ELECTROSTATIC FINITE ELEMENT MODEL

To study the impact of substrate material and ground connection on electric field distribution and intensity, a 3D model of the geometries based on the actual dimensions was designed using COMSOL Multiphysics 5.6. A constant voltage of 2 kV was applied to one pad while another pad was grounded. It was observed that the field intensity for different pad configurations did not vary significantly. However, the presence of a BSG increased the field intensity by a factor of two. Unlike the results without BSG, where the tangential electric field dominates, the electric field intensity with BSG connected is significantly increased (approximately twice the former case), and the vertical component of the electric field becomes dominant.

To demonstrate the impact of the BSG and substrate material on the electric field intensity and distribution lines, the electric field plots in a perpendicular cut plane between the pads of RR geometry are presented in Fig. 15 for two substrates with different permittivity values. By connecting the BSG, higher distortion and concentration of the electric field lines and electrical stress across the dielectric under the high voltage pad are observed. This initial observation of the locally intensified electric field around the high voltage pad clearly explains the lower PDIV values for samples with BSG. However, this electrostatic study does not accurately reveal the impact of the dielectric permittivity on the electric field intensity based on the transient PD results obtained for

two substrates, i.e., AlN and G-10/FR4. The impact of this parameter on the transient behavior of the PD is discussed in the next section.

V. NAVIGATING THE RESULTS LANDSCAPE TOWARDS VALIDATED IMPLICATIONS

A. REFINED COMPUTATIONAL APPROACH: PAIRING NUMERICAL ANALYSIS WITH FINITE ELEMENT MODELING

While local electric field stress is the primary driving factor for PD initiation, it alone cannot fully represent the transient behavior of this phenomenon. Gas ionization, especially in low-pressure air, is crucial for faster charge generation and propagation on dielectric surfaces, potentially causing surface tracking and flashover on PCBs.

To account for this factor in our previous studies [23], [24], we developed an electro-hydrodynamic based streamer model in 2D representation. This model demonstrated how electric field-dependent impact ionization in the gas significantly affects streamer formation in both positive and negative voltage polarities.

However, applying these coupled charge particle partial differential equations (PDEs) as governing relations in a 3D model is computationally challenging. Therefore, to study the impact of gas ionization on surface discharge initiation at low pressures in this work, we have developed a pressure-, temperature-, and electric field-dependent ionization factor (χ). This factor is derived from the aforementioned model and allows for more efficient 3D simulations.

The analytic expression of the pressure and temperature dependent effective ionization factor, derived from Hartmann's empirical formula in [25], is given below:

$$\chi = \bar{\alpha}\left|\overline{W}_e\right| = P\frac{T_0}{T}\left[1.75\times10^3\left(1+\frac{1.15\times10^{-6}}{\left(\frac{|E|}{P}\cdot\frac{T}{T_0}\right)^3}\right)\cdot\exp\left(\frac{-0.04}{\frac{|E|}{P}\cdot\frac{T}{T_0}}\right)-\frac{0.9}{\left[1.49+\exp\left(\frac{P}{587}\cdot\frac{T_0}{T}\right)\right]}\right]\cdot1.3\times10^5\left(\frac{T\,|E|}{P}\right)^{0.74}\quad T_0=273K \tag{1}$$

where $\bar{\alpha}$, $\overline{W}_e$, E, P, and T are effective ionization coefficient in m^{-1}, absolute value of the electron drift velocity vector in $m.s^{-1}$, the electric field in $kV\cdot mm^{-1}$, gas pressure in *Torr*, and gas temperature in *Kelvin*.

The logarithmic values of the electric field-dependent ionization factor given in (1) are plotted for three pressure levels in Fig. 16. The values of 2.37, 0.46, and 0.23 kV/mm at 100, 20, and 10 kPa, respectively, are the activating field points of the curves where the ionization factor has a steep rise from significantly small values (with negative log values) to beyond 10^7 particles per second. More importantly, these plots justify the ratio of the PDIV values obtained from the experiments at different pressures (see Fig. 3 to 8). In a non-uniformly distributed electric field between the pads, the PD is expected to initiate from locations where the impact ionization reaches these activating field points.

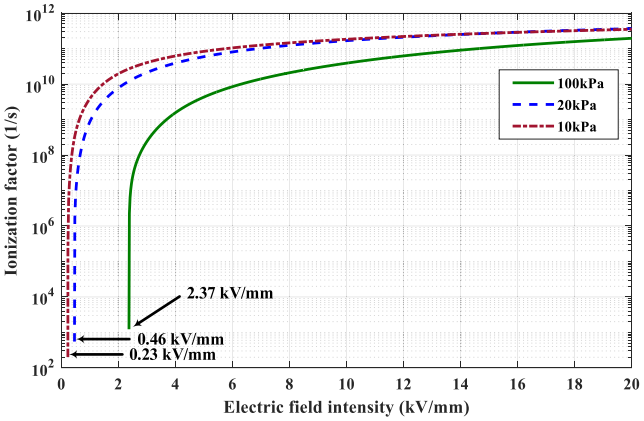

FIGURE 16. Ionization factor versus electric field at different pressures.

To identify the possible location of the PDs for different designs and ionization factor intensities under different pressures, the introduced equation was coupled to the electrostatic equations predefined in the 3D model. Fig. 17 demonstrates the gas ionization around the boundaries of the high voltage pad at different pressures. In all designs, the peak value is at the edges where the electric field intensity is highest.

For LS design, the point 'c' has the lowest value, and the regions between b-c and c-d have higher ionization beyond 10^9 s^{-1} at low pressures. By connecting the BSG, the regions between a-b and d-e are excited as well. For RR design, a similar trend is observed with a constant ionization rate between b-c with a symmetric and uniform electric field intensity. For RS design, the ionization increases in the mid of the b-c line where the ground pad is in close proximity to the HV pad. It can be concluded that the PD is ignited when the ionization factor exceeds 10^8 s^{-1} in Fig. 16. Also, it is expected that the flashover following the PD is observed in these regions. Our observation from the tests confirms this analytical explanation for different designs as shown in Fig. 18.

On the other hand, the gas-filled bubbles impose further electrical stresses on the encapsulated power modules due to the electric field enhancement inside the bubble with lower permittivity compared to the gel. In section I, we presented the prior research work discussing the bubble formation and deformation behavior led by discharge filamentary branched discharge trees. In other words, disregarding the pressure effect, these bubbles are formed due to local field enhancement in front of the discharge branches on the substrate. However, bubbles in our study form at low pressures. They mainly result from incomplete gel attachment to pads and corners of stacked copper plates on substrates. Microscale gaps between pads and substrates can also cause bubbles. These issues lead to higher space charge injection and local electric field enhancement. Low pressure in these weak areas causes swollen gaps and bubble formation. In severe cases,

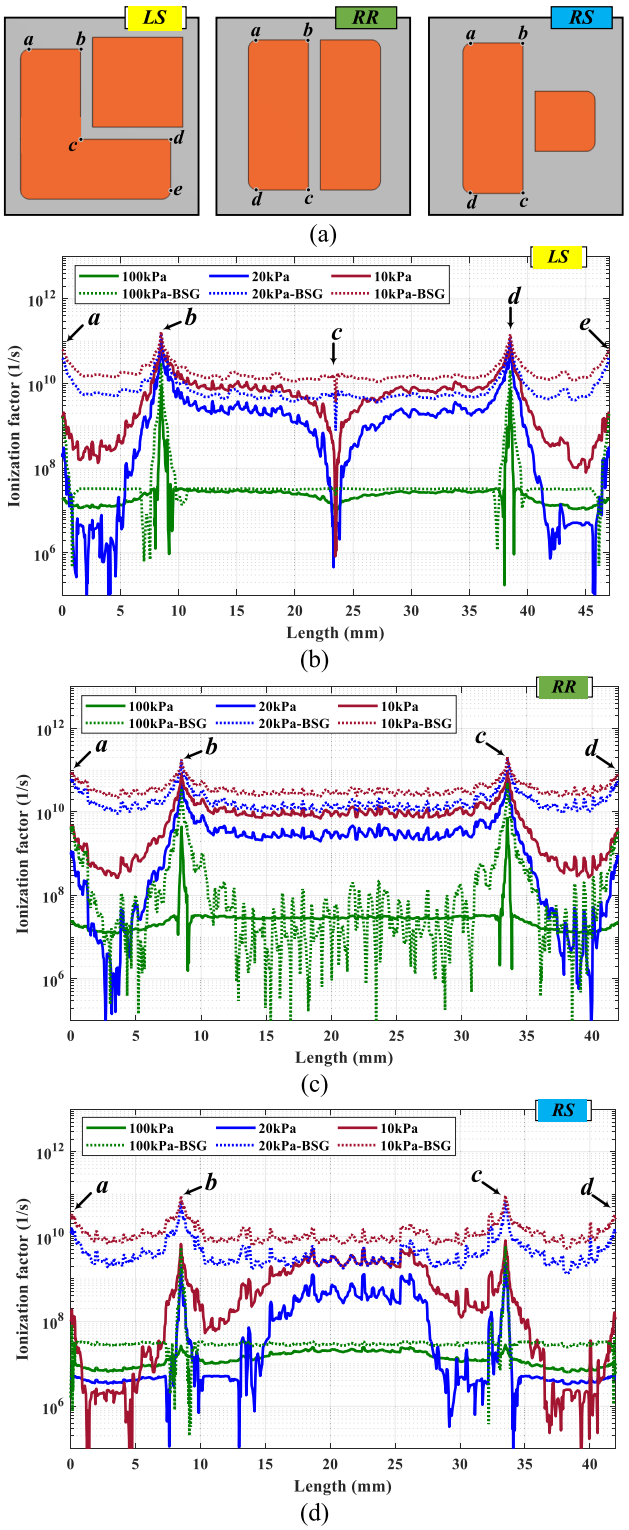

FIGURE 17. The ionization factor plots (a) along the boundaries of high voltage pad adjacent to the ground pad at different pressures for: (b) LS, (c) RR, and (d) RS pad designs with and without BSG.

it can lead to further gel detachment from the substrate. Our recommendations given in subsection II-B can significantly help in avoiding the formation of bubbles bigger than a few millimeters in diameter and the detachment of gels; however, the formation of the bubbles around the pads at low pressures (<20kPa) is inevitable. Fig. 19 shows two typical bubbles formed around the pads at low pressure. Generally speaking, more than 70% of the bubbles disappear when the pressure increases to ambient, while the rest of the bubbles might take up to 12 hours to disappear.

FIGURE 18. Typical location of the observed flashover between the pads for different designs.

FIGURE 19. Typical bubbles formed around the corners of the pads in RR (left) and RS (right) pad designs taken by visible light microscope.

The lower permittivity of these gas-filled bubbles intensifies the local electric field inside the bubble which leads to PD initiation at low voltages. In addition, the low pressure of the gas inside the bubble enclosed by silicone gel, affected by the environment pressure at high altitudes, increases the ionization rate of the atoms and ions as discussed earlier. Borghei and Ghassemi [26] have developed a numerical model to obtain the PRPD patterns for an enclosed void inside a silicone gel for the study of the impact of low pressure on the PD repetition rate. Impact of the pressure has been considered in their PD inception electric field formula introduced by Niemeyer et al [27]. They have shown that the PD repetition rate is doubled at half atmospheric pressure. To accurately scrutinize the impact of the altitude on the gas ionization inside the bubble formed inside the gel as the key influencing factor in the PD initiation, we incorporated the ionization factor formula in (1) in simulated model of bubbles along the substrate between the pads. We studied the impact of the pressure on the proposed ionization factor as the direct indicator of discharge incident inside the gas-filled bubble.

Fig. 20 displays the simulated 3D model in COMSOL Multiphysics 5.6. A highly refined mesh is defined at the bubble locations. This enables accurate calculation of localized electric field intensity inside micro-sized bubbles enclosed by the gel ($\varepsilon_r = 2.85$). It also allows determination of ionization factor values at different locations inside bubbles of varying sizes and positions.

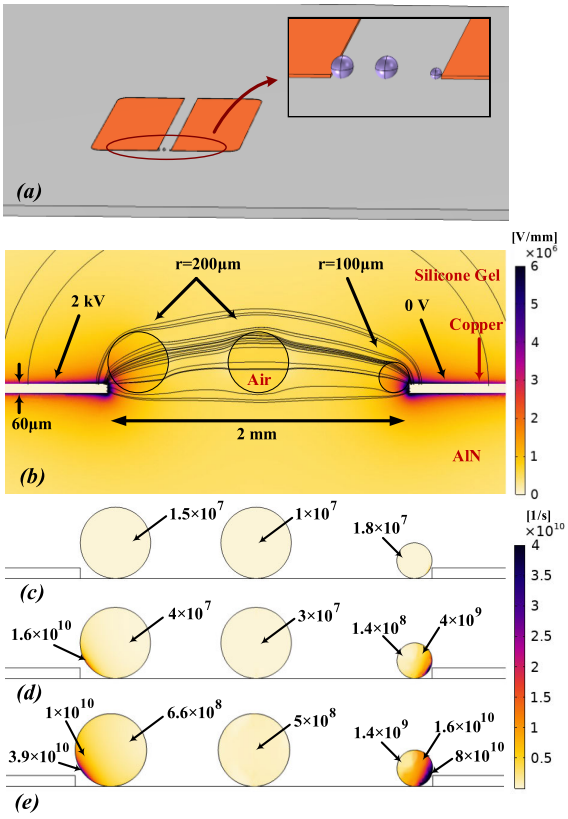

FIGURE 20. 3D Finite element model of (a) multiple spherical bubbles with different sizes at different locations between the RR pads encapsulated by silicone gel: (b) electric field intensity and distribution, and pressure-dependent ionization factor at (c) 100kPa, (d) 20kPa, and (e) 10kPa.

As shown in Fig. 20(b), the closer the bubbles are to the pads and smaller they are, the more intense the electric field inside the bubbles is. Fig. 20(c)-(e) show the impact of the pressure on the ionization factor inside the bubbles as well as the values of this parameter at different locations inside the bubbles. It indicates that the ionization of the gas atoms at 20 and 10 kPa corresponding to the approximate altitudes of 35 and 50 kft can be 1-2 orders of magnitude higher than ambient pressure. As mentioned earlier, the possible chance of bubble formation affects the PDIV results recorded in multiple measurements for the same configuration and gel encapsulant, which can be one of the main reasons behind the wider recorded PDIV values given in Fig. 11-14, compared to the measured values for fluorinert-encapsulated samples presented in Fig. 9 and 10. Also, it is important to note that the surface charge modification across the bubbles and its effect on the local electric field was not considered in this model.

B. PD PATTERN CHARACTERIZATION AND SOURCE IDENTIFICATION

1) NON-ENCAPSULATED SAMPLES: GEOMETRIC DESIGN ISSUES

Two-dimensional PRPD patterns are a well-known visual representation of the PD activity that has been widely used to identify the PD source and its type (e.g., corona, internal, and surface discharges) and have been the main diagram provided by the conventional PD data analyzers for the insulation failure analysis. It visualizes the position of the recorded PD pulse magnitudes in reference to the phase of the applied AC voltage. We have reviewed the distinctive features of these patterns in analyzing the different type of defects for different high voltage apparatus in [28]. Beside the PDIV values recorded and presented in section III, the PD intensity based on the repetition rate (number of PDs per second) and magnitude of the recorded pulses represented in PRPD patterns should be discussed.

Fig. 3 to 8 present the significant reduction in the PDIV values at low pressures (20 and 10 kPa). The recorded PRPD patterns show a lower PD intensity at PDIV under low pressures; however, a small increase of the voltage can lead to high gas ionization and flashover at low pressures. For example, Fig. 21 shows the PRPD patterns recorded for LS geometry.

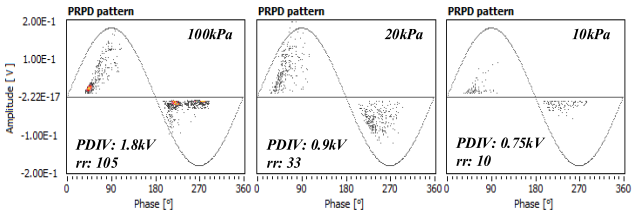

FIGURE 21. PRPD pattern recorded for LS_s_2 on AlN substrate at different pressures (rr: repetition rate).

Although a significant difference was not seen between PDIV values recorded for pads with 2- and 4-mm distances, PDs between the pads with a longer distance, initiated at a higher voltage, have less repetition rate due to the low electric field intensity between the pads. The recorded patterns for RS geometry shown in Fig. 22 exemplify this statement.

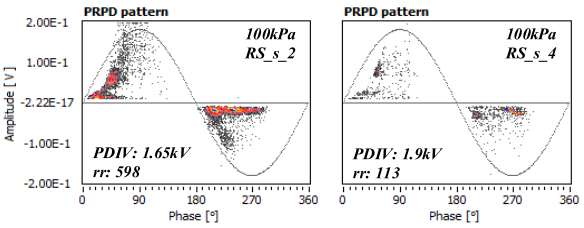

FIGURE 22. PRPD pattern recorded for RS design with different distance between the pads at ambient pressure (rr: repetition rate).

The time-frequency (TF) mapping of the recorded PD waveforms, discussed in our previous research work [29], provides further information when the PD pulse waveforms during the recording time are not similar due to the possible multiple PD sources and locations. The PRPD patterns and TF maps extracted for two different pad geometries shown in Fig. 23 justify the initiation of the PDs at different paths as observed flashover photos in Fig. 18 indicate. PDIV values

for LS and RR pad designs given in Fig. 3 and 5 with 2mm distance and sharp edges are the same and the PRPD pattern in the following figure shows the same PD repetition rate for these designs. The multiple concentrated PD pulse data in their TF maps shown in the right column indicate the multiple PD paths as shown in Fig. 18 for flashover paths. A higher concentration of the PD data can relate to a higher PD intensity at the edges such as highlighted blue region for RR pad design.

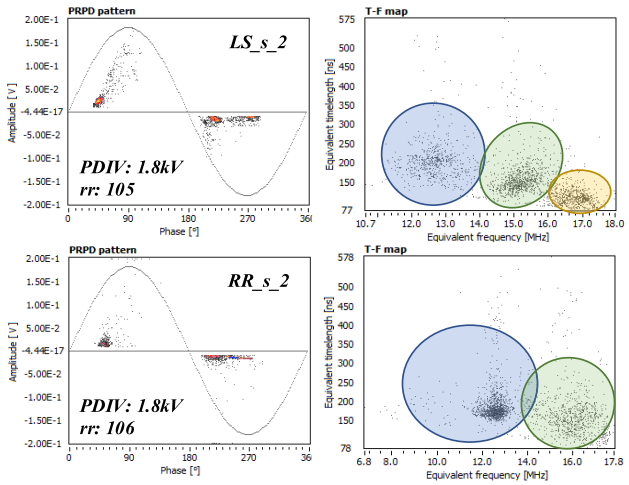

FIGURE 23. PRPD pattern and T-F maps extracted for LS and RR pad designs with the same PDIV values.

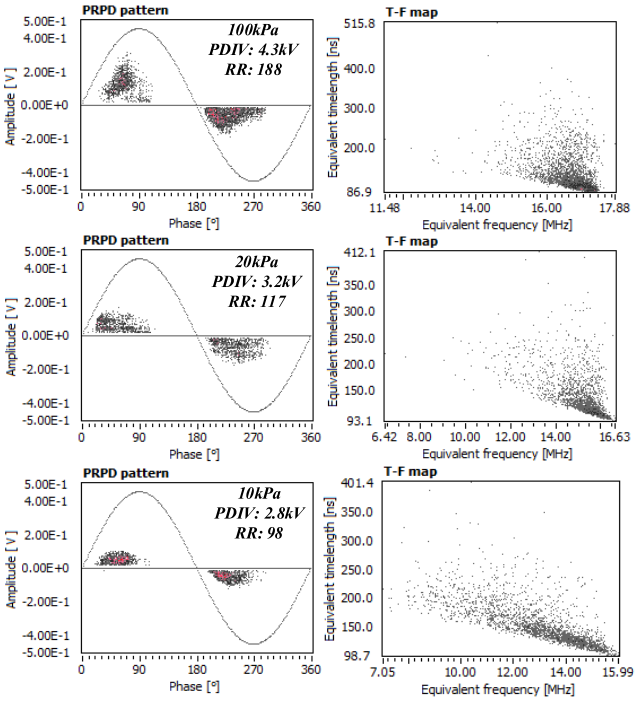

FIGURE 24. PRPD patterns and TF maps for fluorinert-encapsulated LS_4mm pad design without BSG connection at different pressures (RR: repetition rate).

2) ENCAPSULATED SAMPLES WITH INTERNAL DEFECTS

Unlike gel-encapsulated samples, it is rare for bubbles to form in fluorinert-encapsulated samples to lead to the steady weak points igniting the PDs and further degradation of the sample. As discussed in section I, any possibly formed bubbles at low pressures are repelled from the strong electric field area and expelled out of the encapsulant. Therefore, it was expected the discharges to occur on the surface boundary between the fluorinert and substrate where the two materials meet. The consistent PRPD patterns were recorded for the fluorinert-encapsulated samples as a typical result shown in Fig. 24. Patterns show a lower magnitude of the PD pulses and their repetition rate under low applied voltage as pressure drops.

Although the PDIV values reported for both silicone gel encapsulants showed considerable differences, the PRPD patterns are not comparable for the same encapsulated design. However, depending on the likelihood of bubble formation and the location of the PD, the results can be further discussed. Our test results showed a similar PD intensity for three different encapsulants in this study. However, the formation of the bubbles in silicone gel can further intensify the PDs in the localized area and accelerate the degradation of the gel at low pressures. As an example, Fig. 25 shows a typical PD pattern and TF map results obtained for RS pad design with BSG connection encapsulated by SiG 4170. The higher intensity and magnitude of the PDs in these results compared to the results given in Fig. 24 is due to the BSG connection and closer distance between the pads, although the PDIV values are significantly lower as well. As discussed, the electric field intensity between the pads for different studied designs is approximately the same, while the locations of the maximum stress are different. Also, Fig. 25 shows multiple clusters of the data in the TF map as the pressure drops which can be an indication of the formation of multiple PD sources. On the other hand, the repetition rate of the PDs does not decrease as reported for fluorinert, which is a compelling justification for the formation of bubbles between the pads at low pressures and having higher gas ionization inside the gas-filled bubbles.

C. MATERIAL-DRIVEN PD BEHAVIOR ANALYSIS IN SUBSTRATES AND ENCAPSULANTS

1) DIELECTRIC SUBSTRATE

We have used both AlN and G-10/FR4, two main base materials used for power modules and PCBs, as the substrate of the samples to study their impact on the PD behavior recorded for different geometries. The excellent heat dissipation or high heat conduction capability of the AlN, unmatched by FR4, is considered the main advantage of using this material for the power modules to prevent module failure due to thermal stress during the continuous switching of the semiconductor devices [30]. Even so, regarding the electrical stresses, the electrical parameters of the dielectric material such as permittivity and breakdown voltage should be further discussed. Since the capability of the FR4 used as the substrate of PCBs

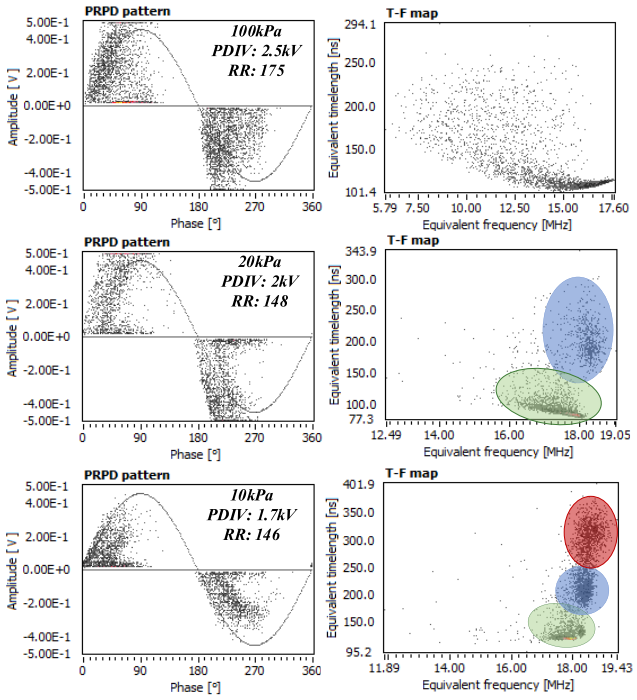

FIGURE 25. PRPD patterns and TF maps for SiG4170-encapsulated RS_2mm pad design with BSG connection at different pressures (RR: repetition rate).

for high voltage application has not been well addressed by other works, and has lower permittivity than AlN, the presented results obtained for different pad geometries shed light on the impact of material permittivity on the PD behavior.

The test results given in Figs. 3, 5, and 7 show higher PDIV values (20-30% at ambient pressure and 10-20% at 20 and 10kPa) for the AlN with higher permittivity than G-10/FR4. The simulation results presented in Fig. 15 from the electrostatic model indicate that the permittivity does not have a significant impact on the electric field distribution and intensity. However, Meng et al. [31] and our previous study on the surface discharge behavior of different dielectric materials [32] indicate the fact that the dielectric material with a higher permittivity produces lower local electric field in front of the streamer branches required for discharge propagation between the electrodes at a fixed applied voltage and reduces their velocity. In other words, a higher voltage is needed to initiate a discharge along a dielectric surface with a higher permittivity.

2) ENCAPSULANT PROPERTIES IN PD MITIGATION

The silicone gel products used in this study not only have higher dielectric strength which makes them good candidates for high-power electronic module encapsulation, but also retain their physical and chemical crosslinked properties at low pressures which is required for aerospace application. However, the effectiveness of both silicone gels and fluid encapsulants in protecting the devices against PD is significantly reduced at low pressures. Our test results presented in section III show comparably higher PDIV values for SiG 527 compared to SiG 4170. Volume resistivity and dielectric constant are the key factors defining the electric field distribution under DC and AC voltages, respectively, which are generally in the same range for these gels at ambient pressure. However, the resistivity of the gel can be affected differently by the reduced pressure. Bubble formation as a result of pressure drop is the main source of internal PD. It is believed the guidelines introduced in this paper can have a significant impact on bubble mitigation at low pressures, however, the surface discharge in the boundary of silicone gel and substrate/pads is another source of recorded PDs which depends on the adhesive bonding of the gel to the substrates/pads and its effectiveness under forces imposed by surrounded low air pressure at high altitudes. Encapsulated samples with SiG527 in this study have comparably higher adhesive strength than SiG4170, which can lend to its superior performance resulting in higher PDIV values for different designs at different pressures compared to Fluorinert and SiG4170.

VI. CONCLUSION

In this comprehensive study, we conducted an in-depth investigation into the complex phenomena of PD and flashover behaviors across three distinct pad geometries. Our research focused on two widely used base dielectric substrates - AlN and G-10/FR4 - which are crucial components in high-voltage power electronics. By initially testing without dielectric encapsulants, we established a fundamental understanding of how pad designs, substrate materials, and BSG connections influence PD at various atmospheric pressure levels. This approach not only revealed the electrically weakest points in the designs but also demonstrated how strategic modifications could significantly alter PD characteristics. Also, we quantified the impact of various parameters on partial discharge initiation and intensity through rigorous experimental methods. Furthermore, we employed advanced numerical simulations to analyze gas ionization within trapped bubbles in encapsulants at higher altitudes, providing valuable insights for applications in aerospace and high-altitude environments. This multifaceted approach bridges the gap between theoretical predictions and practical applications, offering crucial data for the design and optimization of high-voltage power modules in diverse operating conditions. Key conclusions are:

Pad Geometry and Substrate Materials:

- The PDIV values recorded for three main pad geometries with the same distances between the pads are almost the same. The simulation results show the same electric field intensity with different PD locations. Also, the study shows roughly 2 times higher maximum tangential electric field intensity with the BSG copper layer connected.
- The novel analytical model, defined as ionization factor χ, coupled with the 3D model shows that the PDIV can

be increased by up to 1.25 and 1.5 times by smoothing out the pad edges for the design without and with BSG, respectively. Also, the PD intensity is reduced only when the distance between the pads increases.

- PDIV values at 20 and 10kPa are 40-50% and 55-65% lower, respectively, than the values at ambient pressure. The PDIV/flashover values at 10kPa are slightly lower (about 10%) compared to the values at 20kPa. However, the detection of PDIV at low pressures is difficult due to a high gas ionization at low pressure as the proposed ionization factor demonstrated. Also, the undetectable drift of the electrons can be increased at low pressure, and Townsend discharge might be the dominant type of detected discharges between the pads compared to Streamer discharge at low pressures due to the above-mentioned high gas ionization impact.
- The electrostatic study shows a minor impact of the permittivity on the electric field intensity and distribution; however, the transient behavior of the PD is affected by this factor. The PDIV values recorded for AlN substrate with higher permittivity are approximately 10-30% higher than the G-10/FR4.
- The PRPD patterns and T-F maps discussed in this paper provide information about the PD intensity and occurrence of the PD at different locations between the pads.

Encapsulations:

- A 23-27% and 30-36% reduction of PDIV is expected for a fluorinert-encapsulated sample under 20kPa and 10kPa compared to ambient pressure, respectively. The differences are 15-35% and 35-50% for the silicone gel-encapsulated samples.
- Simulation results from a finite element-based 3D model of bubbles with different sizes at different locations indicate that the ionization of the gas atoms at 20 and 10kPa can be 1-2 orders of magnitude higher than ambient pressure. The closer the bubbles are to the pads and smaller they are, the more intense the electric field inside the bubbles is.
- Generally, 10-50% lower PDIV values were obtained for gel-encapsulated G-10/FR4 compared to the AlN substrate.
- Presence of the bubbles between the pads and multiple active PD sources can be detected through clustered data in the T-F map plot and the intensity/repetition rate of PRPD patterns at different pressures.
- Higher PDIV values for SiG527 compared to SiG4170 can be due to limited surface discharge activity in the boundary of gel and substrate/pad for this sample with higher adhesion. SiG527 likely achieves better adhesion to the tested substrates, combine with a balance of the key gel properties, associated with cross-linking and hardness; the self-healing quality whilst providing dimensional stability of a dielectric elastomer. However, a thorough further analysis is required to determine which of these properties is most impactful.

REFERENCES

[1] V. Madonna, P. Giangrande, and M. Galea, "Electrical power generation in aircraft: Review, challenges, and opportunities," *IEEE Trans. Transport. Electrific.*, vol. 4, no. 3, pp. 646–659, Sep. 2018.
[2] G. Buticchi, P. Wheeler, and D. Boroyevich, "The more-electric aircraft and beyond," *Proc. IEEE*, vol. 111, no. 4, pp. 356–370, Apr. 2023.
[3] *Electrical Power Systems*, INSIGHT, U.K. Aerosp. Technol. Inst. HQ, Cranfield, U.K., 2018.
[4] T. Ueda, "Reliability issues in GaN and SiC power devices," in *Proc. IEEE Int. Rel. Phys. Symp.*, Jun. 2014, pp. 3D.4.1–3D.4.6.
[5] C. Qian, A. M. Gheitaghy, J. Fan, H. Tang, B. Sun, H. Ye, and G. Zhang, "Thermal management on IGBT power electronic devices and modules," *IEEE Access*, vol. 6, pp. 12868–12884, 2018.
[6] F. Yan, L. Wang, Y. Gan, K. Li, and B. Zhang, "A new structure of ceramic substrate to reduce the critical electric field in high voltage power modules," *J. Electron. Packag.*, vol. 144, no. 3, Sep. 2022, Art. no. 031016, doi: 10.1115/1.4053891.
[7] L. Wang, Z. Zeng, P. Sun, S. Ai, J. Zhang, and Y. Wang, "Electric-field-dominated partial discharge in medium voltage SiC power module packaging: Model, mechanism, reshaping, and assessment," *IEEE Trans. Power Electron.*, vol. 37, no. 5, pp. 5422–5432, May 2022.
[8] Y. Yang, L. Dorn-Gomba, R. Rodriguez, C. Mak, and A. Emadi, "Automotive power module packaging: Current status and future trends," *IEEE Access*, vol. 8, pp. 160126–160144, 2020, doi: 10.1109/ACCESS.2020.3019775.
[9] Y. Liu, *Power Electronic Packaging: Design, Assembly Process, Reliability and Modeling*. New York, NY, USA: Springer, 2012.
[10] B. Wang, J. Cai, X. Du, and L. Zhou, "Review of power semiconductor device reliability for power converters," *CPSS Trans. Power Electron. Appl.*, vol. 2, no. 2, pp. 101–117, 2017, doi: 10.24295/CPSST-PEA.2017.00011.
[11] L. M. Salvatierra, L. I. Kovalevski, P. L. D. Quiña, I. M. Irurzun, E. E. Mola, S. J. Dodd, and L. A. Dissado, "Self-healing during electrical treeing: A feature of the two-phase liquid-solid nature of silicone gels," *IEEE Trans. Dielectr. Electr. Insul.*, vol. 23, no. 2, pp. 757–767, Apr. 2016.
[12] P. Mancinelli, A. Cavallini, S. J. Dodd, N. M. Chalashkanov, and L. A. Dissado, "Analysis of electrical tree inception in silicone gels," *IEEE Trans. Dielectr. Electr. Insul.*, vol. 24, no. 6, pp. 3974–3984, Dec. 2017.
[13] S. Nakamura, A. Kumada, K. Hidaka, M. Sato, Y. Hayase, S. Takano, K. Yamashiro, and T. Takano, "Electrical treeing in silicone gel under repetitive voltage impulses," *IEEE Trans. Dielectr. Electr. Insul.*, vol. 26, no. 6, pp. 1919–1925, Dec. 2019.
[14] M. Sato, A. Kumada, K. Hidaka, K. Yamashiro, Y. Hayase, and T. Takano, "Viscoelastic analysis of cavity propagation in gel with electrical discharge," *J. Phys. D, Appl. Phys.*, vol. 47, no. 15, Apr. 2014, Art. no. 155201.
[15] I. Semenov, I. F. Gunheim, K. Niayesh, H. K. H. Meyer, and L. Lundgaard, "Investigation of partial discharges in AlN substrates under fast transient voltages," *IEEE Trans. Dielectr. Electr. Insul.*, vol. 29, no. 2, pp. 745–752, Apr. 2022.
[16] J.-L. Auge, O. Lesaint, and A. T. V. Thi, "Partial discharges in ceramic substrates embedded in liquids and gels," *IEEE Trans. Dielectr. Electr. Insul.*, vol. 20, no. 1, pp. 262–274, Feb. 2013.
[17] J.-H. Fabian, S. Hartmann, and A. Hamidi, "Analysis of insulation failure modes in high power IGBT modules," in *Proc. 40th IAS Annu. Meeting. Conf. Rec. Ind. Appl. Conf.*, vol. 2, 2005, pp. 799–805.
[18] T. Lebey, D. Malec, S. Dinculescu, V. Costan, F. Breit, and E. Dutarde, "Partial discharges phenomenon in high voltage power modules," *IEEE Trans. Dielectr. Electr. Insul.*, vol. 13, no. 4, pp. 810–819, Aug. 2006.
[19] T. Shahsavarian, D. Zhang, P. McGinnis, S. Walker, Z. Zhang, and Y. Cao, "Altitude readiness of high-voltage IGBTs subjected to the partial discharge at harsh environmental conditions for hybrid electric aircraft propulsion," *IEEE Trans. Power Electron.*, vol. 37, no. 4, pp. 3733–3736, Apr. 2022.
[20] S. J. Dodd, L. Salvatierra, L. A. Dissado, and E. Mola, "Electrical trees in silicone gel: A combination of liquid and solid behaviour patterns," in *Proc. Annu. Rep. Conf. Electr. Insul. Dielectr. Phenomena*, Oct. 2013, pp. 1018–1021.
[21] Y. Xu, B. Luo, F. Zhang, and X. Zeng, "Investigation on discharge pattern of fluorinated liquid under boiling condition," in *Proc. IEEE Int. Conf. High Voltage Eng. Appl. (ICHVE)*, Sep. 2020, pp. 1–4.
[22] A. F. Junior and D. J. Shanafield, "Thermal conductivity of polycrystalline aluminum nitride," *Ceramica*, vol. 50, pp. 247–253, Sep. 2004.

[23] T. Shahsavarian and Y. Cao, "An inventive multi-scale, multiphysics modeling approach and comparative analysis of distinctive features of planar ionization waves in air: I. Negative streamers," *J. Phys. D, Appl. Phys.*, vol. 55, no. 24, Jun. 2022, Art. no. 245203.
[24] T. Shahsavarian and Y. Cao, "An inventive multi-scale, multiphysics modelling approach and comparative analysis of distinctive features of planar ionization waves in air: II. Positive streamers," *J. Phys. D, Appl. Phys.*, vol. 55, no. 24, Jun. 2022, Art. no. 245204.
[25] G. Hartmann, "Theoretical evaluation of peek's law," *IEEE Trans. Ind. Appl.*, vol. IA-20, no. 6, pp. 1647–1651, Nov. 1984.
[26] M. Borghei and M. Ghassemi, "Characterization of partial discharge activities in WBG power converters under low-pressure condition," *Energies*, vol. 14, no. 17, p. 5394, Aug. 2021.
[27] L. Niemeyer, "A generalized approach to partial discharge modeling," *IEEE Trans. Dielectr. Electr. Insul.*, vol. 2, no. 4, pp. 510–528, Aug. 1995.
[28] T. Shahsavarian, Y. Pan, Z. Zhang, C. Pan, H. Naderiallaf, J. Guo, C. Li, and Y. Cao, "A review of knowledge-based defect identification via PRPD patterns in high voltage apparatus," *IEEE Access*, vol. 9, pp. 77705–77728, 2021.
[29] T. Shahsavarian, C. Li, M. A. Baferani, and Y. Cao, "Surface discharge studies of insulation materials in aviation power system under DC voltage," in *Proc. IEEE Conf. Electr. Insul. Dielectr. Phenomena (CEIDP)*, Oct. 2020, pp. 271–274.
[30] S. Kalker, L. A. Ruppert, C. H. van der Broeck, J. Kuprat, M. Andresen, T. A. Polom, M. Liserre, and R. W. De Doncker, "Reviewing thermal-monitoring techniques for smart power modules," *IEEE J. Emerg. Sel. Topics Power Electron.*, vol. 10, no. 2, pp. 1326–1341, Apr. 2022.
[31] X. Meng, H. Mei, C. Chen, L. Wang, Z. Guan, and J. Zhou, "Characteristics of streamer propagation along the insulation surface: Influence of dielectric material," *IEEE Trans. Dielectr. Electr. Insul.*, vol. 22, no. 2, pp. 1193–1203, Apr. 2015.
[32] T. Shahsavarian, X. Wu, C. Lents, D. Zhang, C. Li, and Y. Cao, "Temperature-dependent partial discharge characteristics of high temperature materials at DC voltage for hybrid propulsion systems," *High Voltage*, vol. 6, no. 4, pp. 590–598, Aug. 2021.

TOHID SHAHSAVARIAN (Member, IEEE) received the bachelor's degree in electrical engineering from the University of Tabriz, in 2011, the master's degree from Iran University of Science and Technology (IUST), in 2013, and the Ph.D. degree in electrical engineering from the University of Connecticut. He has conducted research on electrical insulation enhancement, partial discharge, and numerical and finite element modeling for electrical and power electronic components. His work supported projects for NASA, the U.S. Navy, Raytheon Technologies Corporation, Collins Aerospace, and the Eversource Energy Center. Currently, he is an Expert Engineer and a Technical Lead with PG&E, specializing in the new technology evaluation and its integration into T&D power grid projects, failure root cause analysis, and partial discharge consulting for a variety of PG&E assets, including new and aged underground cables and rotating machines. He has authored over 35 peer-reviewed journal and conference papers. His research interests include partial discharge analysis and risk assessment, high voltage testing of AC and DC high power apparatus, and reliability analysis and protection of HVAC/HVDC grids for utilities and aerospace applications.

MORITZ PLONER (Graduate Student Member, IEEE) received the B.Sc. degree in electrical engineering from Vienna University of Technology, Austria, in 2020, and the M.Sc. degree in electrical energy engineering from the University of Bologna, Italy, in 2022. He is currently pursuing the Ph.D. degree in advanced-systems engineering with the Free University of Bozen–Bolzano, Italy, in collaboration with Empatica, a full-stack digital healthcare company and pioneer in continuous health monitoring. His research focuses on designing flexible electrochemical sensors for wearable applications to detect human biochemical profiles from sweat.

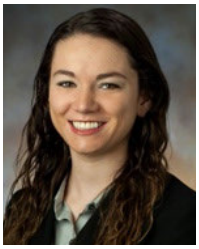

KERRY LYNN DAVIS-AMENDOLA (Graduate Student Member, IEEE) received the B.S. and M.S. degrees from the University of Connecticut, Storrs, CT, USA, in 2016 and 2023, respectively. She is the Adhesives and Elastomers Engineering Manager with Pratt and Whitney. She holds five U.S. patents, has authored or co-authored 12 publications, and studies materials for the aerospace industry.

BRIAN CHISLEA joined Dow Chemical Company, in 2004, as a Compound Semi-Conductor Associate and later promoted to a Scientist and an Application Engineer. He is passionate about EV development, advancing charging technology, and improving reliability.

JOHN MCKEEN received the Ph.D. degree in chemical engineering from California Institute of Technology, in 2009. He is currently the Technical Director with Dow Chemical Company, leading the global mobility and transportation technical service and development organization for Dow Performance Silicones. With a team of more than 85 engineers, scientists, and technicians, he and his colleagues focused on innovation and collaboration to serve the material needs of the mobility and transportation industry, including thermally and electrically conductive silicones for thermal and EMI management of electronic components and assemblies; silicone conformal coatings, encapsulants, gels, and pottants to enable reliable electronics; adhesives for assembly; coatings for airbags, synthetic leather, and aerospace applications; silicone foams; optically clear silicones for injection molding and encapsulation; and high consistency (HCR) and liquid (LSR) silicone rubbers for a range of applications.

DI ZHANG (Fellow, IEEE) is a Full Professor with the Naval Postgraduate School. He has ten years of cutting-edge industrial research and development experience in electric power and energy areas, including the applications for high/medium voltage transmission and distribution electric power systems for land/marine/aviation applications, electric motor drives, smart/micro grids, renewable energy and oil and gas, and energy storage. In addition, he has more than five years teaching and researching experience in academia for Navy power system. He is the author of 36 issued U.S. patents, more than 30 journal articles, 27 conference papers, and one book chapter.

ANDREA CAVALLINI (Fellow, IEEE) is a Full Professor with the Department of Electrical, Electronic, and Information Engineering ''Guglielmo Marconi,'' University of Bologna, works on endurance modeling and diagnostics of insulation systems. His research focuses on partial discharges detection and identification through innovative detection system and artificial intelligence techniques. His current principal line of investigation is partial discharge phenomena under PWM voltage waveforms. In particular, the dependence of partial discharge phenomena on thermal aging, temperature, and pressure, is dealt due to its strong impact in the automotive and aerospace industry. He is also involved in the characterization of dielectrics and electrical insulation systems for power electronics. He is the co-author of about 280 scientific papers and 15 international patents and a co-founder of the university spin-off Techimp. He is active in IEEE DEIS, CIGRE (an Italian National Representative (2004–2008) and a Convener of WG D1.43 and D1.74), IEC TC 2 MT 10 (a Project Leader of IEC 60034-18-41 Ed. 2), and SAE (WG AE11).

YANG CAO (Senior Member, IEEE) received the B.S. and M.S. degrees in physics from Tongji University, Shanghai, China, and the Ph.D. degree from the University of Connecticut, in 2002. After that, he was a Senior Electrical Engineer with the GE Global Research Center, until 2013. He is currently a Full Professor with the Electrical and Computer Engineering Department, University of Connecticut. He is also the Director of the Electrical Insulation Research Center, Institute of Materials Science; and the Site Director of the NSF iUCRC Center on High Voltage/Temperature Materials and Structures. His research interests include the physics of materials under extremely high field and the development of new dielectric materials, particularly the polymeric nanostructured materials for energy efficient power conversion and renewables integrations and novel medical diagnostic imaging devices.